J. COMBIN. MATH. COMBIN. COMPUT. 127b (2025) 2819--2832

Journal of Combinatorial Mathematics
and Combinatorial Computing
www.combinatorialpress.com/jcmcc

Combinatorial Press

Modeling and simulation of permafrost changes in the upper Irtysh River basin driven by meteorological data based on partial differential equations

Ting Kong[1], Shuai Li[2], Pu Zhang[1,✉], Qinglei Li[3], Weiping Liu[1], Qiwen Wang[1]

[1] *Xinjiang Meteorological Information Center, Urumqi, Xinjiang, 830002, China*
[2] *The Lightning Protection Center of Xinjiang Uygur Autonomous Region, Urumqi, Xinjiang, 830002, China*
[3] *National Meteorological Information Center, Beijing, 100081, China*

ABSTRACT
The study of the impact of climate change on permafrost and the response mechanism in the Upper Irtysh River Basin can help to comprehensively understand the impact of climate change and grasp the development of coping strategies. In this paper, the one-dimensional heat conduction equation is used as the core to propose a model for calculating the distribution of permafrost in the upper Irtysh River Basin and the boundary conditions for solving the model, and the model is simulated and solved by using the general form of partial differential equations in the COMSOL Multiphysics finite element analysis software. Subsequently, the simulation results and regression equations are combined to investigate the driving effect of meteorological data changes on permafrost depth distribution changes. The simulation results found that the meteorological factor regression model could explain 30.6% of the variation in maximum permafrost depth, with mean annual relative humidity driving permafrost depth to the greatest extent (Beta = -0.251). This paper finds that the driving effect of meteorological factors on permafrost depth change provides a new perspective for understanding the dynamical mechanism of permafrost change in the upper Irtysh River Basin, and also provides a scientific basis for predicting and responding to the impact of future climate change on permafrost.

Keywords: COMSOL software, partial differential equation, regression analysis, meteorological factors, permafrost depth modeling

1. Introduction

The Irtysh River is - a transnational river, originating from the southern slopes of Altay Mountains in Fuyun County, Xinjiang Uygur Autonomous Region, China, located in the mid-latitude of the Northern Hemisphere, the prevailing westerly circulation area, the climate from the Atlantic Ocean is easy to

✉ Corresponding author.
E-mail address: 18963817495@sohu.com (P. Zhang).
Received 10 January 2024; Revised 25 May 2024; Accepted 20 October 2024; Published Online 16 April 2025.
DOI: 10.61091/jcmcc127b-159

enter into the region through the Irtysh River valley, and subject to the mountainous uplift, which creates richer precipitation in the mountainous areas [1]. The basin is subject to high evaporation due to spring gales, and evaporation increases with decreasing elevation from the mountains to the plains [2]. The basin is located in the hinterland of the Asian and European continents, far from the sea, with typical continental cold-temperate climate characteristics, with long and severe winters and short and cool summers [3]. In this context, there are sufficient conditions for the formation of permafrost zone in the basin, but in recent years, due to global climate change and human activities, permafrost changes in the Irtysh River basin are complicated.

Permafrost is soil or rock containing ice, which is commonly found at high latitudes and high altitudes [4]. The existence of permafrost is related to factors such as temperature, soil type, topography and vegetation, and is an important part of the Earth's surface processes and material cycles. Cold climates are the basic conditions for the formation and development of permafrost, and in cold climates, the water in the soil freezes at low temperatures, forming permafrost [5]. The mountains and hills in high latitudes are relatively higher and cooler, not only the rainfall is higher, the water to form permafrost is more abundant, so the severity and duration of the cold climate and the cycle of freezing and thawing also affect the size of the depth of permafrost [6-7]. In addition, under rainfall conditions, the surface layer of permafrost is easily washed away by rainwater due to the erosive effect of rainwater, leading to soil erosion, which carries away particles from the surface of permafrost, exacerbating the degradation and destruction of permafrost [8-9]. For permafrost, its solid phase is not only soil particles, but also a new solid phase material-ice formed by freezing of soil solution. And rainfall can infiltrate into permafrost and freeze further, leading to an increase in the water content of permafrost, which in turn enhances the stability of permafrost [10]. At the same time, rainfall can increase the humidity of permafrost, which serves to regulate the temperature of permafrost by releasing a large amount of latent heat [11]. In addition, permafrost can have an important effect on the morphology and geomorphology of the land. The process of freezing and thawing of permafrost causes the ground to undulate and settle, forming typical traces of freeze-thaw land formation and subsurface freezing and thawing, whereas intense rainfall may lead to accelerated thawing of permafrost, which may cause geologic hazards such as mudslides and landslides [12-14]. On the contrary, climate warming leads to increased permafrost thawing, and since permafrost is one of the largest carbon reservoirs on earth, storing a large amount of organic matter, which is decomposed by bacteria and fungi, releasing a large amount of greenhouse gases such as carbon dioxide and methane, which further aggravate the greenhouse effect and global warming, as well as releasing hazardous substances such as mercury [15-18]. This positive feedback effect can lead to accelerated climate change. Normally, permafrost acts as a ground support, but when permafrost thaws, the water in the soil is dissipated, leading to a reduction in soil volume, which in turn triggers soil subsidence [19-21]. This poses a great challenge to infrastructure development and ecosystem stabilization, in permafrost areas. Buildings and roads may be damaged, and flowing groundwater can alter wetlands and rivers in a thousand different ways. In mountainous areas, thawing permafrost may lead to large-scale landslides and mudslides, as well as the release of pathogenic bacteria that threaten the safety of people's lives and property, which not only poses a great disaster risk to local residents, but also causes serious damage to ecosystems such as water resources, forests, and biodiversity [22-24]. These conditions have brought great difficulties and challenges to land use and construction, and have had a significant impact on local vegetation, animal husbandry, fisheries, agriculture, and transportation networks [25-28].

In this paper, a multi-year permafrost depth distribution calculation model is constructed for the upper Irtysh River basin based on the one-dimensional heat conduction equation, and the study area of the Irtysh River basin is decomposed into a number of pixels, and the distribution of permafrost depth in the region is simulated based on the soil temperature, volumetric heat capacity, and soil clay grain content in each pixel. Subsequently, the model was inputted into COMSOL Multiphysics finite element analysis software, and the general form partial differential equations of the PDE module of the software were used to realize the simulation and solution of the model of permafrost depth distribution change. In this study, the meteorological factor data and permafrost depth distribution data collected from six observation stations in the Irtysh River basin were statistically analyzed. The accuracy-tested partial differential equation model was used to simulate the future meteorological factors and permafrost depth data in the study area, and finally the regression equation was used to analyze the degree of influence of each meteorological factor on the driving influence of permafrost depth in the upper Irtysh River basin.

2. Method

2.1. Modeling of permafrost changes

2.1.1. Model description. The core of the perennial permafrost distribution model is the one-dimensional heat transfer equation [29], which reflects the dynamics of perennial permafrost by simulating the soil temperature. The study area is discretized into images of $1km \times 1km$. In each image, only the heat flow in the vertical direction is considered, thus solving for the soil column under each image. The model assumes that the variation of internal energy and temperature at the surface is completely determined by Fourier's law of heat conduction [30]. The model is defined as follows:

$$C\frac{\partial T}{\partial t} = \frac{\partial}{\partial y}\left(k\frac{\partial T}{\partial y}\right) \tag{1}$$

where C is the volumetric heat capacity of the soil $\left(Jm^{-3}℃^{-1}\right)$, k is the thermal conductivity of the soil $\left(Wm^{-1}℃^{-1}\right)$, y is the depth down to the surface (m), T is the soil temperature (℃), t is the time (days).

The model also takes into account the differences in the volumetric heat capacity and thermal conductivity of the soil in different freeze-thaw states, as well as the influence of the latent heat of phase change on the simulation results, which is expressed as:

$$C = \begin{cases} C_f & T < T_e - \Delta T \\ C_f + L_w \dfrac{\theta - \theta_u}{\Delta T} & T_e - \Delta T \le T \le T_e \\ C_u & T > T_e \end{cases} \tag{2}$$

$$k = \begin{cases} k_f & T < T_e - \Delta T \\ k_f + \dfrac{k_u - k_f}{\Delta T}\left[T - \left(T_e - \Delta T\right)\right] & T_e - \Delta T \le T \le T_e \\ k_u & T > T_e \end{cases} \tag{3}$$

where f and u subscripts denote the frozen and unfrozen states, respectively, $L_w = 334.5MJkg^{-1}$ is the latent heat of phase transition of ice and water, θ and θ_u are the saturated water content of the soil and the volumetric unfrozen water content, respectively $\left(m^3m^{-3}\right)$, T_e is the onset freezing temperature, set to -0.01°C, and ΔT is the interval in which the phase transition occurs set to 0.5°C.

2.1.2. Soil parameters. Parameters applied in the model include volumetric heat capacity, thermal conductivity, volumetric water content and volumetric unfrozen water content in the freeze-thaw state. When soil water freezes, the water close to the soil particles remains in the liquid state due to absorptive and capillary forces exerted by the soil particles. This kind of results in melting and freezing of ice in contact with soil particles occurring over a range of temperatures rather than at different temperatures. The presence of unfrozen water alters the thermal and hydrologic properties of the soil. Neglecting unfrozen water in the model leads to large uncertainties in the estimation of soil temperatures. A parameterization that defines the liquid water content of frozen soils as a soil matrix potential function has been widely used in many recent surface models. The hydraulic conductivity coefficient and soil matrix potential (ψ, mm) vary with volumetric water content and soil texture. When ice is present, the soil water potential is in disequilibrium with the vapor pressure over pure ice, and the soil matrix potential for each soil layer can be expressed when the soil water infiltration potential is neglected:

$$\psi(T) = \frac{10^3 L_w (T - T_e)}{gT} \tag{4}$$

where g is the gravitational acceleration. The relationship between soil matrix potential and unfrozen water is:

$$\psi(\theta_u) = \psi_{sat} \left(\frac{\theta_u}{\theta_{sat}} \right)^{-b} \tag{5}$$

where θ_{sat} is the soil porosity and ψ_{sat} is the soil matrix potential at saturation calculated from the content of sand in the soil:

$$\Psi_{sat} = -10 \times 10^{1.88 - 0.0131\theta_{sand}} \tag{6}$$

b is the Clapp-Hornberger parameter, calculated from soil clay content:

$$b = 2.91 + 0.159 * \theta_{clay} \tag{7}$$

where θ_{sand} is the soil sand content $(m^3 m^{-3})$ and θ_{clay} is the soil clay content $(m^3 m^{-3})$.

Combining Eqs. (4) to (6) the unfrozen water content is derived as:

$$\theta_u = \theta_{sat} \left\{ \frac{10^3 L_w (T - T_e)}{gT\Psi_{sat}} \right\}^{-\frac{1}{b}} \tag{8}$$

2.1.3. Model boundary setting. The upper boundary of the model was set at the ground surface (defined as 0m), and the driving data were the average of daytime and nighttime surface temperatures from the day-by-day 1km all-weather surface temperature dataset in western China. The lower boundary of the model was set at 100m depth, with a temperature gradient of 0.03°C/m in the study area based on previous findings, and the heat flux calculated from the thermal conductivity at 100m depth as the lower boundary condition.

2.1.4. Calculation of freezing and thawing indices. Freezing and thawing indices are important indicators of changes in the thermal state of the surface in cold regions at high latitudes. The annual freezing index and thawing index can be used to assess the distribution of perennial and seasonal permafrost, the depth of freezing of soil, and changes in the thickness of the active layer. In this study, surface temperature was used to calculate the freezing index and thawing index. The surface freezing index refers to the accumulation of surface temperatures less than 0°C in the cold season, which is generally calculated from July 1 to June 30 of the following year, and the surface thawing index refers to the accumulation of surface temperatures greater than 0°C in the warm season, which is calculated from January 1 to December 31st. Therefore, its calculation formula is:

$$FI = \sum_{i=1}^{N} |T_i|, T_i < 0℃ \tag{9}$$

$$TI = \sum_{i=1}^{N} |T_i|, T_i > 0℃ \tag{10}$$

where FI is the surface freezing index, TI is the surface thawing index, T_i is the surface temperature, and N is the calculated time.

2.2. Model solving and simulation methods

2.2.1. COMSOL Multiphysics Fundamentals. COMSOL Multiphysics is a finite element software that simulates realistic physical phenomena by solving partial differential equations [31]. The advantage of COMSOL Multiphysics is that it can couple multiple physical fields by solving systems of partial differential equations discretely, and the software is a powerful environment that can be used for modeling and solving a wide range of scientific and engineering problems. The software provides a powerful desktop environment and a model generator that allows the user to have a comprehensive understanding of the model and access to all functions. Another advantage of COMSOL is that the user does not need strong knowledge of mathematical or numerical analysis to easily extend a regular class of physical models into multi-physics field models for solving coupled physical phenomena. By using the built-in physical interfaces and defining material properties, the user can construct equations directly by defining relevant physical quantities (e.g., material properties, loads, constraints, fluxes, sources, etc.) instead of defining the underlying equations, and apply these variables, expressions, or numbers directly to the solid or fluid domain, independently of the computational mesh, and after that the software will internally compile a set of equations that represent the entire model automatically. Equations. When solving the model, COMSOL uses an advanced set of numerical analysis tools to assemble and solve the equations. The software runs the analysis using a variety of numerical solvers along with adaptive meshing (user-selected) and error control, and these studies can take advantage of multiprocessor systems and cluster computation, as well as batch processing and parameter scanning. COMSOL documents all the steps in the creation of the geometry, meshing, study and solver setup, as well as visualization and representation of the results, by creating sequences. This makes it easy to change any part of the parametric model, and facilitates the user to adjust the created numerical model. COMSOL applications include, among others, acoustics, biological sciences, chemical reactions, diffusion, fluid dynamics, geophysics and geomechanics, heat transfer, corrosion and corrosion protection, multibody dynamics, optics, particle tracking, photonics, porous media flow, structural mechanics, quantum mechanics, wave propagation, etc. Many practical applications involve the simultaneous coupling of multiple physical fields, and the software has provided predefined interfaces for common multi-physical field coupling, which is convenient for users to call. And in the basic configuration of the software, prefabricated modules are provided for many fields, which simplify the creation and analysis of models. Meanwhile, the PDE module is also set up to allow users to input various types of partial differential equations or systems of partial differential equations for modeling and solving according to their own needs, which greatly improves the operability.

2.2.2. Partial Differential Covariance Based Model Simulation. The PDE module in COMSOL provides coefficient form, general form, and a weak form partial differential form distinct from the geometric hierarchy. These three interfaces can solve any user-defined second-order partial differential equations. The weak form is the most basic form, which is closely related to the finite element theory, and the coefficient form as well as the general form of partial differential equations are transformed to the weak form inside the software, so the choice of which type of interface for partial differential equations depends mainly on the fact that the use of which type of equations is more convenient and can be more easily specified in a particular form. In this paper, general form partial differential equations were chosen to implement the simulation and analysis of meteorological and permafrost data.

The General Form Partial Differential Equations module provides a generic interface [32] for specifying and solving partial differential equations in a general form, a format that is closely related to conservation laws that control many areas of physics. If a single dependent variable u is used, the expression for the partial differential equation in general form is as follows:

$$\begin{cases} e_a \dfrac{\partial^2 u}{\partial t^2} + d_a \dfrac{\partial u}{\partial t} + \nabla \cdot \Gamma = f, in\Omega \\ -n \cdot \Gamma = g - qu + h^T \mu, on\partial\Omega \\ 0 = R, on\partial\Omega_c \\ u = r, on\partial\Omega_d \end{cases} \tag{11}$$

where Ω is the computational domain, the concatenation of all domains, $\partial\Omega$ is the domain boundary, and n is the unit normal vector outward on $\partial\Omega$. The first term is a partial differential equation satisfying domain Ω, and the second, third, and fourth terms are boundary conditions. The second term is the general form of the Neumann boundary condition, also known as the natural boundary condition because it does not appear explicitly in weak form in the partial differential equation problem, and in the software partial differential equation interface the corresponding boundary is called the flux or source, which specifies the value of the boundary out numerical flux Γ. The third term is the general constraint, also known as the fundamental boundary condition in finite element theory, which specifies that any expression is equal to zero on the boundary. The fourth term is the Dirichlet boundary condition, which is a special form of the third general constraint that directly specifies the value of the dependent variable at the boundary, which makes the constraint a more general boundary condition.

Γ, f, g, q, R, and r are user-defined coefficients that can be functions of spatial coordinates, spatial derivatives of solutions u or u, or other predefined and user-defined variables. The coefficients f, g, q, r, R are scalars and Γ is a flux vector.

3. Results and discussion

3.1. Overview of the study area

The study area is located in the upper reaches of the Irtysh River, which originates from Qigertai Darshan in the northern part of Fuyun County, Xinjiang Uygur Autonomous Region, China, and is the only river in China that flows into the Arctic Ocean. The Irtysh River is a seasonally frozen river, with bank ice beginning to appear around October each year, freezing in December, and a freezing period of about 120 to 160 days until the river opens completely in early May of the following year. Perennial permafrost and seasonal permafrost are common in the Irtysh River basin, and the critical elevation of perennial permafrost and seasonal permafrost is 2200m, and the elevation of the selected sites in the study area is lower than 2200m.

3.2. Station Observed Meteorological and Permafrost Change Data

3.2.1. Basic information on observation sites. Station observations in the Upper Irtysh River Basin area consist of two types of data: automatic weather observing stations and ground stations. The automated weather station data come from the climate monitoring array established by the United States Geological Survey (USGS), including one automated weather station. Ground station data come from the Circumpolar Activity (CALM) monitoring network, which consists of five ground stations. Specific data information for the six observing stations in the Upper Irtysh River Basin area is shown in Table 1.Meteorological data such as air temperature, snow depth, humidity, soil temperature, soil moisture, and soil thaw depth were used in this study along with permafrost data parameters.

Table 1. Research area observation station information

Site name	Site number	Year	Latitude (°N)	Longitude (°E)	Elevation (m)
Haba	U1	1958-2021	48.52	86.23	532.6
Gaki	U2	1961-2021	47.44	85.87	984.1
Bolsu	U3	1960-2021	47.29	87.42	473.9
Fuhai	U4	1961-2021	45.62	88.52	497.0
Arlear	U5	1955-2021	47.21	88.23	735.3
Richness	U6	1957-2021	45.23	89.21	807.5

3.2.2. Analysis of changes in meteorological data at observation points:

1) Meteorological data analysis. In this study, two types of temperature data were collected from both automatic weather stations and ground sites. The automatic weather station was monitored using a CSI 107 thermistor probe in a radiation shield located 3.5 m above the ground surface. Data were averaged hourly after every 60 seconds of data collection. To minimize errors, voltages were converted to temperature values in data processing using a four-period calibration function suitable for temperatures ranging from -50°C to 30°C. For ground station data, OnsetTM type thermistor data loggers are used to collect data at 30-minute, 1-hour, or 2-hour intervals, with an effective temperature range of -50°C to 30°C and a resolution of about 0.32°C. The data are then converted into temperature values using a four-period calibration function. Snowpack data are snow depth data obtained from automatic weather observation stations. Snow depth was measured hourly with a CSI SR50 ultrasonic distance sensor mounted approximately 3.1 m above the ground surface. The results of the analysis of the temperature change data at the six observation stations in the upper Irtysh River basin under study are shown in Fig. 1, with (a)-(f) representing the results of the temperature changes at the Habahe, Jimunai, Burzin, Fuhai, Altay, and Fuyun observation stations, respectively. The mean annual temperatures at the six sites in 2021 were 6.2°C, 5.4°C, 5.6°C, 5.5°C, 5.4°C and 5.3°C, respectively. The annual maximum and annual minimum temperatures at the Habahe observation site in 2021 were among the highest among the studied sites, with 12°C and 0.9°C, respectively.

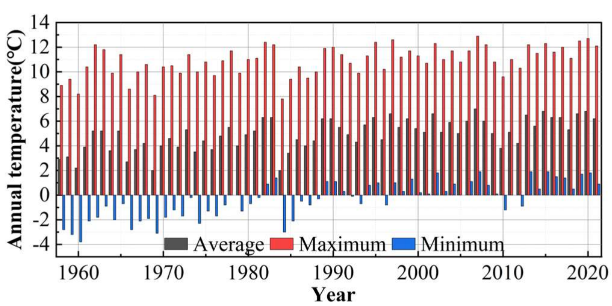

(a) Haba

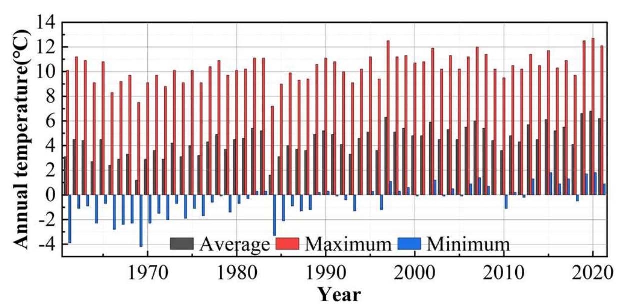

(b) Gaki

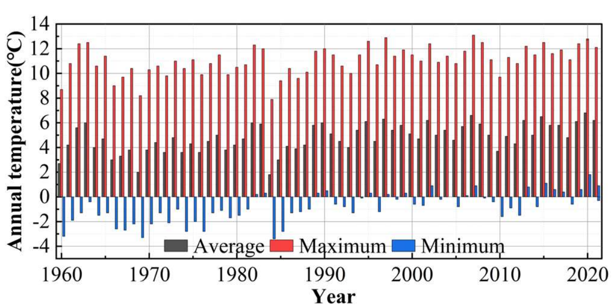

(c) Bolsu

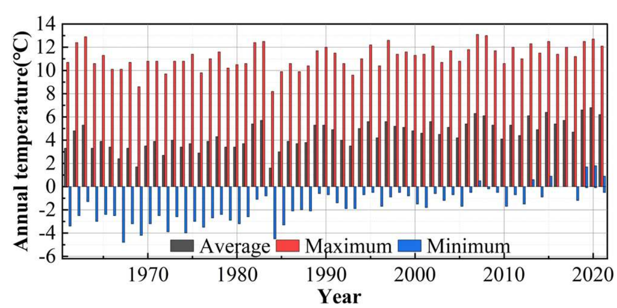

(d) Fuhai

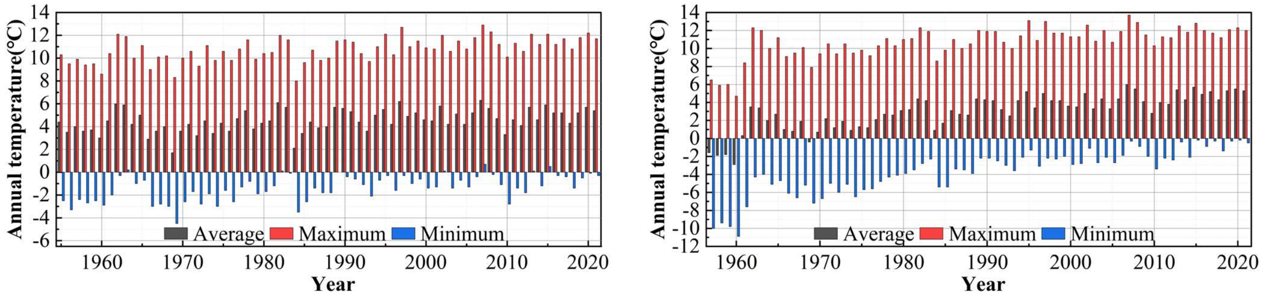

(e) Arlear (f) Richness

Fig. 1. Temperature analysis results

The analyzed data of meteorological factors such as precipitation, humidity and wind speed at the observation stations in the study area are shown in Table 2. Precipitation in the Upper Irtysh River Basin was low during the study period, and the annual average total precipitation at the six stations ranged from 145.1 mm to 213.0 mm, with the number of days without precipitation at the observation site in Burqin reaching 195 days, and precipitation was mainly concentrated in the months of September-November. The relative humidity varied greatly in the upper Irtysh River basin area, and in terms of annual average relative humidity, the highest average relative humidity was 62.6% at the Burzin observation site. The study period was perennially windy, with annual mean wind speeds ranging from 1.8 m/s to 3.8 m/s.

Table 2. Analysis of meteorological factors such as humidity and wind speed

Site name	Year	Numerical value	Precipitation (mm)	Humidity (%)	Snow depth (cm)	Wind speed (m/s)
Haba	1958-2021	Max	359.7	66.0	67.0	5.2
		Min	90.1	56.0	4.0	2.5
		Average	198.3	60.5	21.7	3.8
Gaki	1961-2021	Max	363.5	64.0	75.0	5.1
		Min	109.8	52.0	11.0	2.3
		Average	213.0	57.2	29.8	3.6
Bolsu	1960-2021	Max	280.8	67.0	58.0	5.4
		Min	58.2	57.0	4.0	2.4
		Average	145.1	62.6	19.6	3.8
Fuhai	1961-2021	Max	215.0	67.0	47.0	3.6
		Min	42.3	56.0	6.0	1.8
		Average	125.3	61.9	16.5	2.6
Arlear	1955-2021	Max	338.5	64.0	94.0	3.2
		Min	76.4	50.0	17.0	1.5
		Average	200.3	58.1	44.5	2.2
Richness	1957-2021	Max	398.6	68.0	89.0	2.7
		Min	83.4	53.0	9.0	0.6
		Average	203.2	59.2	38.9	1.8

3.2.3. Analysis of permafrost depth distribution. Analyzing the temporal and spatial variation data of the maximum permafrost depth in the upper Irtysh River basin, significant temporal and spatial differences in the maximum permafrost depth at different stations over the years were obtained. The results of the analysis of permafrost depth distribution are shown in Fig. 2, with (a)-(f) representing the results of permafrost depth changes at Habahe, Jimunai, Burzin, Fuhai, Altay and Fuyun observatories, respectively. From the time dimension, it seems that the maximum depth of permafrost fluctuates greatly at each station in different years, e.g., the maximum depth of permafrost at the Jimunai station ranges from 87 cm to 202 cm, that at the Burzin station ranges from 48 cm to 127 cm, and that the maximum depth of permafrost at the Fuyumi station and the Altay station ranges between 74 cm-169 cm and 56 cm-146 cm. This proves that there are large interannual variations in permafrost depth in the upper Irtysh River basin between different years. In terms of spatial variation, the maximum permafrost depth at each site also has obvious geographical differences. For example, the maximum permafrost depth at the Jimunai site may be much smaller than that at the Fuyun site in some years, while the opposite is true in other years. The existence of spatial differences is related to a variety of factors such as geographic location, topography, and climatic conditions. In addition, by calculating the average of the maximum permafrost depths of the six stations over the years, it can be found that the maximum permafrost depths of the Upper Irtysh River Basin as a whole also show certain fluctuating trends.

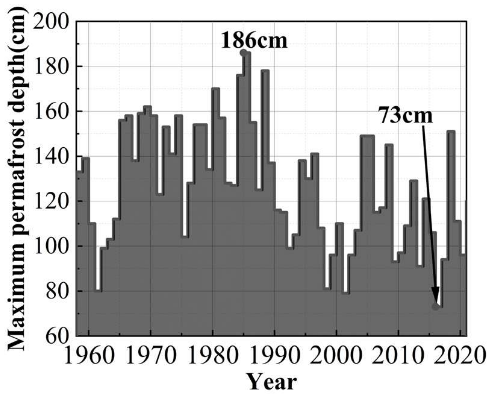

(a) Haba

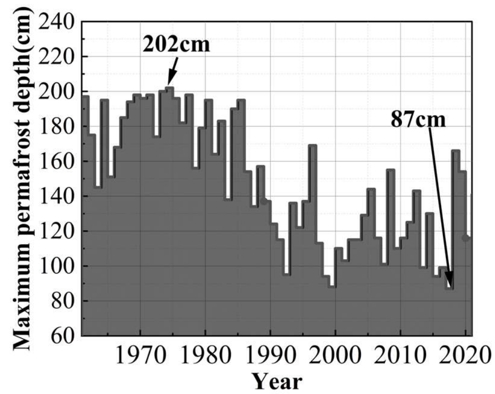

(b) Gaki

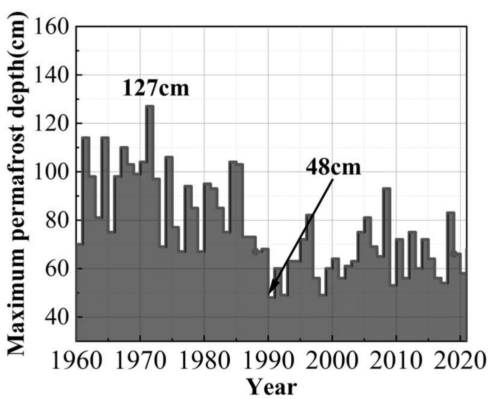

(c) Bolsu

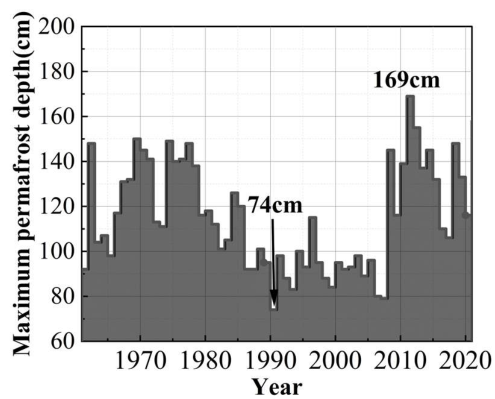

(d) Fuhai

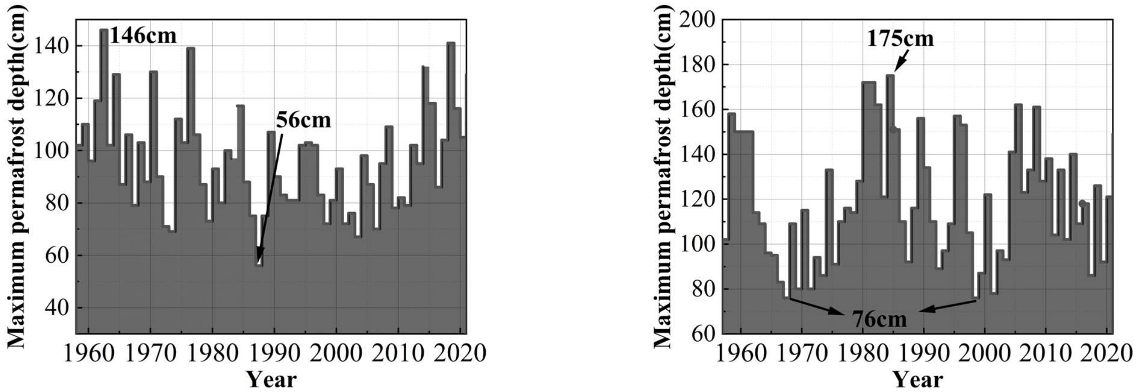

(e) Arlear (f) Richness

Fig. 2. The largest permafrost depth in the region of the Erzs river

3.3. Simulation analysis of the relationship between meteorology and permafrost changes

3.3.1. Accuracy test of model simulation results. Root mean square error (RMSE), mean absolute error (MAE), and coefficient of determination (R^2) were chosen as evaluation indexes to report the simulation performance of each model and to assess the model accuracy.RMSE is used to measure the deviation between simulated and observed values, and MAE represents the average of the absolute errors between predicted and observed values, and the smaller the values of both, the higher the model prediction accuracy. R^2 reflects the degree of fit between predicted and observed values, and the closer R^2 is to 1, the better the model has the goodness of fit and the higher the accuracy of prediction. The formula is as follows:

$$RMSE = \sqrt{\frac{1}{n}\sum_{i=1}^{n}\left(y_i - \hat{y}_i\right)^2} \tag{12}$$

$$MAE = \frac{1}{n}\sum_{i=1}^{n}\left|\left(y_i - \hat{y}_i\right)\right| \tag{13}$$

$$R^2 = 1 - \frac{\sum_{i=1}^{n}\left(y_i - \hat{y}_i\right)^2}{\sum_{i=1}^{n}\left(y_i - \overline{y}_i\right)^2} \tag{14}$$

where n is the total number of observations, y is the observed value, $\overline{y}$ is the average value of observations, and $\hat{y}$ is the simulated value.

According to the existing meteorological factor data and permafrost distribution depth data of the six observation stations in the upper Irtysh River basin in 2021, the results of the meteorological data error analysis based on the simulation analysis of partial differential equations are shown in Table 3, and the results of the permafrost depth distribution error are shown in Table 4. From the point of view of the simulated and real errors of the meteorological data, the average RSME and MAE values of the simulated data of the six stations of the temperature factor are 0.53°C and 0.10°C, respectively, and R^2 is 0.83. The average absolute error between the simulated data of the rainfall and the real values of the six stations is in the range of 15.0mm-23.2mm, and the average R^2 is 0.82, which is at a higher level, showing that The accuracy of the meteorological data simulated by the partial differential equations of the PDE module in COMSOL is high, which can be applied to the subsequent research. Meanwhile, the simulation of permafrost depth data also showed good simulation accuracy, with average RSME, MAE and R^2 values of 5.93 cm, 5.15 cm and 0.83, respectively.

Table 3. Data simulation results (Permafrost data)

Site name		Haba	Gaki	Bolsu	Fuhai	Arlear	Richness	Average
Temperature	RMSE (℃)	0.9	0.1	0.9	0	0.3	1	0.53
	R^2	0.83	0.83	0.82	0.8	0.84	0.83	0.83
	MAE (℃)	0.1	0	0.1	0.1	0.2	0.1	0.10
Precipitation	RMSE (mm)	16.1	14.5	17.2	16.2	28.9	18.6	18.58
	R^2	0.8	0.84	0.81	0.83	0.81	0.83	0.82
	MAE (mm)	19.2	23.2	15.4	19.9	20.4	15	18.85
Humidity	RMSE (%)	0.35	0.28	0.4	0.38	0.33	0.22	0.33
	R^2	0.83	0.8	0.79	0.85	0.84	0.84	0.83
	MAE (%)	0.34	0.29	0.15	0.21	0.21	0.16	0.23
Wind speed	RMSE (m/s)	0.24	0.81	0.48	0.36	0.3	0.29	0.41
	R^2	0.81	0.79	0.81	0.84	0.81	0.84	0.82
	MAE (m/s)	0.74	0.5	0.04	0.61	0.54	0.48	0.49
Snow depth	RMSE (cm)	1.82	2.6	2.25	2.11	2.66	1.55	2.17
	R^2	0.84	0.84	0.82	0.82	0.83	0.79	0.82
	MAE (cm)	2.04	1.96	2.41	2.75	1.81	2.43	2.23

Table 4. Data simulation results (Meteorological data)

Site name	RMSE (cm)	R^2	MAE (cm)
Haba	4	0.83	6
Gaki	4.6	0.85	2.1
Bolsu	4.1	0.79	7.7
Fuhai	4.2	0.84	3.2
Arlear	8.7	0.84	3.6
Richness	10	0.82	8.3
Average	5.93	0.83	5.15

3.3.2. Analysis of meteorological drivers of permafrost change. Meteorological data and permafrost change data in the Upper Irtysh River Basin were used as inputs to the partial differential equation to simulate and predict the future driving effect of meteorology on permafrost change in the Upper Irtysh River Basin, and linear regression methods were used to calculate the degree of influence of each meteorological factor variable on the maximum freezing depth in the Upper Irtysh River Basin. The results of the regression analysis are shown in Table 5, and the F-test of the model ($F=22.631$, $P=0.000<0.05$) indicates that the model passes the F-test and is ultimately valid. The model can explain 30.6% of the variation in maximum permafrost depth. Judging from the absolute value of Beta coefficient the influence of each meteorological variable on the maximum permafrost depth ranking the larger the absolute value, the greater the driving effect.

Table 5. Regression analysis

——	Nonnormalized coefficient		Normalization factor	t	P
	B	Standard error	Beta		
Constant	-0.003	0.048	——	-0.015	0.956
Annual average temperature	-0.126	0.025	-0.125	-7.526	0.000
Annual precipitation	0.058	0.029	0.048	2.563	0.002
Average annual relative humidity	-0.263	0.024	-0.251	-11.263	0.000
Annual depth	-0.154	0.028	-0.126	-6.325	0.001

Annual average wind speed	0.116	0.029	0.085	4.635	0.006
R^2	0.306				
Adjust R^2	0.298				
F	F(7.362)=22.631,P=0.000				

4. Conclusion

In this paper, the one-dimensional heat conduction equation and Fourier's law of heat conduction are used as the theoretical basis to construct a model for calculating the distribution of permafrost depth in the upper basin of the Irtysh River, and then the simulation and analysis of permafrost changes are realized based on partial differential equations. The meteorological data and permafrost depth data of six observation stations were selected, and it was found that the highest (12℃) and lowest temperature (0.9℃) in 2021 were found in the Haba River observation point in the upper Irtysh River basin. Moreover, the relative humidity varied more in the region of the Upper Irtysh River Basin, and the mean annual wind speed (1.8 m/s-3.8 m/s) was also higher. As for the analysis of permafrost depth, it was found that the maximum permafrost depth of each site also had obvious geographical differences, in which the maximum permafrost depths of the Jimunai site and the Burzin site were in the range of 87cm-202cm and 48cm-127cm, respectively. In addition, the analysis results of partial differential equations and regression equations showed that the meteorological factor regression model could explain 30.6% of the variation of the maximum permafrost depth, indicating that the meteorological changes in the upper Irtysh River Basin have a greater driving effect on the permafrost changes, which can help to predict the trend of the future climate change impact on the permafrost depth.

Funding

This study was supported by Special Project for the Construction of Innovation Environment in the Autonomous Region-Construction of Resource Sharing Platform (PT2323); The Third Xinjiang Scientific Expedition Program (Grant No.2021xjkk1300)"; Guided project of the Xinjiang Uygur Autonomous Region Meteorological Service (YD2022020).

References

[1] Radelyuk, I., Zhang, L., Assanov, D., Maratova, G., & Tussupova, K. (2022). A state-of-the-art and future perspectives of transboundary rivers in the cold climate–a systematic review of Irtysh River. Journal of Hydrology: Regional Studies, 42, 101173.

[2] Fan, J., Abudumanan, A., Wang, L., Zhou, D., Wang, Z., & Liu, H. (2023). Dynamic Assessment and Sustainability Strategies of Ecological Security in the Irtysh River Basin of Xinjiang, China. Chinese Geographical Science, 33(3).

[3] Ma, Y., Zheng, D., Zhang, H., Pang, J., Wang, W., Wang, Y., ... & Xu, S. (2021). Plio-Pleistocene Establishment of Irtysh River in Junggar, Northwest China: Implications for Siberian-Arctic River System Evolution and Resulting Climate Impact. Geophysical Research Letters, 48(12), e2021GL093217.

[4] Li, X., Li, X., & Liu, J. (2024). A dynamic soil freezing characteristic curve model for frozen soil. Journal of Rock Mechanics and Geotechnical Engineering, 16(8), 3339-3352.

[5] Karpenko, F. S., Kutergin, V. N., Dernova, E. O., & Osokin, A. A. (2022). Methods of Studying the Properties of Frozen Soils and Prediction of Their Changes. Water Resources, 49(Suppl 2), S69-S75.

[6] Luo, S., Fang, X., Lyu, S., Jiang, Q., & Wang, J. (2017). Interdecadal changes in the freeze depth and period of frozen soil on the Three Rivers Source Region in China from 1960 to 2014. Advances in Meteorology, 2017(1), 5931467.

[7] Ren, J., & Vanapalli, S. K. (2020). Effect of freeze–thaw cycling on the soil-freezing characteristic curve of five Canadian soils. Vadose Zone Journal, 19(1), e20039.

[8] Ke, Y., Chen, Y., Jiang, Z., & Qiu, Y. (2021). Rainfall erosion damage of residual soil slope in intermittently frozen area based on discrete element method. Frontiers in Materials, 8, 705453.

[9] Hung, C. Y., & Whalen, J. K. (2020). Biophysical controls on nitrous oxide emissions following rain-induced thawing of frozen soil microcosms by simulated rainfall. Soil Biology and Biochemistry, 149, 107960.

[10] Zhou, Z., Zhou, F., Zhang, M., Lei, B., & Ma, A. (2023). Effects of seasonal rainfall variations on the hydrothermal state and thermal stability of the permafrost active layer in the central Qinghai-Tibet Plateau of China. Cold Regions Science and Technology, 214, 103945.

[11] Zhirkov, A., Permyakov, P., Wen, Z., & Kirillin, A. (2021). Influence of rainfall changes on the temperature regime of permafrost in Central Yakutia. Land, 10(11), 1230.

[12] Hao, J., Jia, P., Wu, T., Li, W., Chen, J., Yang, X., ... & Zhang, M. (2023). Numerical analysis of the impacts of rainfall on permafrost-related slope stability on the Qinghai–Tibet Plateau. Journal of Hydrology: Regional Studies, 47, 101439.

[13] Julia, S. (2019). Landslides in permafrost zone of Russia. Landslides: Theory, Practice and Modelling, 303-313.

[14] Baselt, I., & Heinze, T. (2021). Rain, snow and frozen soil: Open questions from a porescale perspective with implications for geohazards. Geosciences, 11(9), 375.

[15] Zhang, Z., Li, M., Wen, Z., Yin, Z., Tang, Y., Gao, S., & Wu, Q. (2023). Degraded frozen soil and reduced frost heave in China due to climate warming. Science of the Total Environment, 893, 164914.

[16] Ban, Y., Lei, T., Chen, C., Yin, Z., & Qian, D. (2017). Meltwater erosion process of frozen soil as affected by thawed depth under concentrated flow in high altitude and cold regions. Earth Surface Processes and Landforms, 42(13), 2139-2146.

[17] Neumann, R. B., Moorberg, C. J., Lundquist, J. D., Turner, J. C., Waldrop, M. P., McFarland, J. W., ... & Turetsky, M. R. (2019). Warming effects of spring rainfall increase methane emissions from thawing permafrost. Geophysical Research Letters, 46(3), 1393-1401.

[18] Schaefer, K., Elshorbany, Y., Jafarov, E., Schuster, P. F., Striegl, R. G., Wickland, K. P., & Sunderland, E. M. (2020). Potential impacts of mercury released from thawing permafrost. Nature communications, 11(1), 4650.

[19] Li, T., Chen, Y. Z., Han, L. J., Cheng, L. H., Lv, Y. H., Fu, B. J., ... & Wu, X. (2021). Shortened duration and reduced area of frozen soil in the Northern Hemisphere. The Innovation, 2(3).

[20] Ming, J., Zhao, Y., Wu, Q., He, H., & Gao, L. (2022). Soil temperature dynamics and freezing processes for biocrustal soils in frozen soil regions on the Qinghai–tibet plateau. Geoderma, 409, 115655.

[21] Wang, X., & Chen, R. (2024). Freezing and thawing characteristics of seasonally frozen ground across China. Geoderma, 448, 116966.

[22] Chen, H., Gao, X., & Wang, Q. (2023). Research progress and prospect of frozen soil engineering disasters. Cold Regions Science and Technology, 212, 103901.

[23] Schuur, E. A., & Mack, M. C. (2018). Ecological response to permafrost thaw and consequences for local and global ecosystem services. Annual review of ecology, evolution, and systematics, 49(1), 279-301.Polar Science, 26, 100589.

[24] Zhang, B., Zhang, B., Xu, Y., Yan, X., Wang, S., Yang, X., ... & Liu, G. (2024). Shift in potential pathogenic bacteria during permafrost degradation on the Qinghai-Tibet Plateau. Science of The Total Environment, 954, 176778.

[25] Revich, B. A., Eliseev, D. O., & Shaposhnikov, D. A. (2022). Risks for public health and social infrastructure in Russian Arctic under climate change and permafrost degradation. Atmosphere, 13(4), 532.

[26] Suleymanov, A. A., Lytkin, V. M., Vinokurova, L. I., Grigoryev, S. A., & Fedorov, S. I. (2023). Rural Communities of Yakutia in Conditions of Permafrost Degradation: Key Risks, Social Consequences, and Adaptation Mechanisms. Arctic, (52), 168-195.

[27] Ward Jones, M., Habeck, J. O., Ulrich, M., Crate, S., Gannon, G., Schwoerer, T., ... & Borchard, N. (2024). Socioecological dynamics of diverse global permafrost-agroecosystems under environmental change. Arctic, Antarctic, and Alpine Research, 56(1), 2356067.

[28] Jin, X., Jin, H., Luo, D., Sheng, Y., Wu, Q., Wu, J., ... & Li, Y. (2022). Impacts of permafrost degradation on hydrology and vegetation in the source area of the Yellow River on Northeastern Qinghai-Tibet Plateau, Southwest China. Frontiers in Earth Science, 10, 845824.

[29] Saumya Ranjan Jena & Archana Senapati. (2024). Explicit and implicit numerical investigations of one-dimensional heat equation based on spline collocation and Thomas algorithm. Soft Computing(20), 12227-12248.

[30] Alzahrani Mohammad Salem J & Alghamdi Najat A. (2023). The vibration of a nanobeam subjected to constant magnetic field and ramp-type heat under non-Fourier heat conduction law based on the Lord-Shulman model. Advances in Mechanical Engineering(5).

[31] Yixin Luo,Dongsheng Chen,Chen Zhang,Jinkun Yang,Tian Gao & Xiaojing Luo. (2025). Simulation of Interface Characteristics and Charge Transfer Dynamics for Layered Electrodes Using Cascade Capacitance in Supercapacitors by COMSOL Software. Journal of chemical information and modeling.

[32] Peng, Linyu. (2022). A modified formal Lagrangian formulation for general differential equations. Japan Journal of Industrial and Applied Mathematics(2),1-26.